



Received 30 November 2023

Accepted 19 January 2024

Edited by N. Alvarez Failache, Universidad de la República, Uruguay

This article is part of a collection of articles to commemorate the founding of the African Crystallographic Association and the 75th anniversary of the IUCr.

**Keywords:** crystal structure; pyrazole; C—H... $\pi$ (ring) interaction; hydrogen bond.

**CCDC reference:** 2327436

**Supporting information:** this article has supporting information at journals.iucr.org/e

# Crystal structure, Hirshfeld surface analysis, crystal voids, interaction energy calculations and energy frameworks and DFT calculations of ethyl 2-cyano-3-(3-hydroxy-5-methyl-1*H*-pyrazol-4-yl)-3-phenylpropanoate

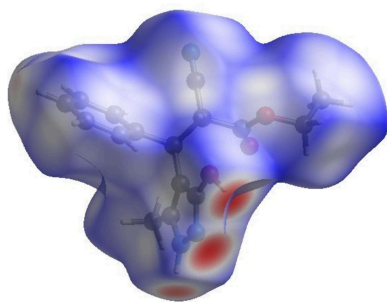
Younesse Ait Elmachkouri,<sup>a,\*</sup> Ezaddine Irrou,<sup>a</sup> Hanae El Monfalouti,<sup>b</sup> Ahmed Mazzah,<sup>c</sup> Tuncer Hökelek,<sup>d</sup> Joel T. Magee,<sup>e</sup> Mohamed Labd Taha<sup>a</sup> and Nada Kheira Sebbar<sup>a,b</sup>

<sup>a</sup>Laboratory of Organic and Physical Chemistry, Applied Bioorganic Chemistry Team, Faculty of Sciences, Ibn Zohr University, Agadir, Morocco, <sup>b</sup>Laboratory of Plant Chemistry, Organic and Bioorganic Synthesis, Faculty of Sciences, Mohammed V University in Rabat, 4 Avenue Ibn Battouta BP 1014 RP, Morocco, <sup>c</sup>University of Lille, CNRS, UAR 3290, MSAP, Miniaturization for Synthesis, Analysis and Proteomics, F-59000 Lille, France, <sup>d</sup>Department of Physics, Hacettepe University, 06800 Beytepe, Ankara, Türkiye, and <sup>e</sup>Department of Chemistry, Tulane University, New Orleans, LA 70118, USA. \*Correspondence e-mail: younesse.aitelmachkouri@edu.uiz.ac.ma

The title compound, C<sub>16</sub>H<sub>17</sub>N<sub>3</sub>O<sub>3</sub>, is racemic as it crystallizes in a centrosymmetric space group (*P* $\bar{1}$ ), although the *trans* disposition of substituents about the central C—C bond is established. The five- and six-membered rings are oriented at a dihedral angle of 75.88 (8)°. In the crystal, N—H...N hydrogen bonds form chains of molecules extending along the *c*-axis direction that are connected by inversion-related pairs of O—H...N into ribbons. The ribbons are linked by C—H... $\pi$ (ring) interactions, forming layers parallel to the *ab* plane. A Hirshfeld surface analysis indicates that the most important contributions for the crystal packing are from H...H (45.9%), H...N/N...H (23.3%), H...C/C...H (16.2%) and H...O/O...H (12.3%) interactions. Hydrogen bonding and van der Waals interactions are the dominant interactions in the crystal packing. The volume of the crystal voids and the percentage of free space were calculated to be 100.94 Å<sup>3</sup> and 13.20%, showing that there is no large cavity in the crystal packing. Evaluation of the electrostatic, dispersion and total energy frameworks indicates that the stabilization is dominated by the electrostatic energy contributions in the title compound. Moreover, the DFT-optimized structure at the B3LYP/6-311 G(d,p) level is compared with the experimentally determined molecular structure in the solid state. The HOMO–LUMO behaviour was elucidated to determine the energy gap.

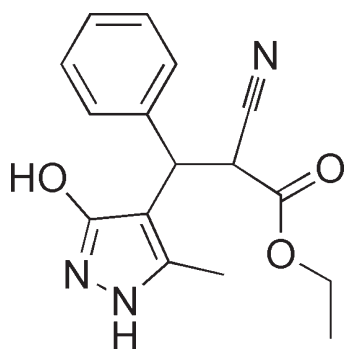
## 1. Chemical context

As part of our ongoing investigation into the use of pyrazoles to develop new heterocyclic systems (Moukha-Chafiq *et al.*, 2006; Elmachkouri *et al.*, 2022; Moukha-Chafiq *et al.*, 2007a; Irrou *et al.*, 2022), particularly those likely to exhibit intriguing biological activities, we note that compounds sharing structural similarities with pyrazole have demonstrated potential in various biological domains, exhibiting analgesic (Gursoy *et al.*, 2000), antifungal and antibacterial (Prasath *et al.*, 2015; Akbas *et al.*, 2005), antiviral (Moukha-Chafiq *et al.*, 2007b) and anticancer (Bensaber *et al.*, 2014) activities. Consequently, the development of innovative synthetic pathways aims to obtain new molecules with structures that are better adapted to cellular receptors. In this respect, we recently reported the synthesis of some pyranopyrazoles (Ait Elmachkouri *et al.*, 2023a) and pyrazolopyranopyrimidines (Ait Elmachkouri *et*



Published under a CC BY 4.0 licence

*al.*, 2023*b*). In our ongoing research, we focus our interest on pyrazole derivatives and present there the synthesis of ethyl 2-cyano-3-(3-hydroxy-5-methyl-1*H*-pyrazol-4-yl)-3-phenylpropanoate, (I). For this synthesis, we adopted a three-component approach, using 3-methyl-1*H*-pyrazol-5-ol, ethyl 2-cyanoacetate and benzaldehyde in ethanol in the presence of piperidine as base. Additionally, we conducted a Hirshfeld surface analysis and performed calculations on intermolecular interaction energies and energy frameworks. We compared the molecular structure optimized using density functional theory (DFT) at the B3LYP/6-311G(d,p) level, with the experimentally determined molecular structure in its solid state.



## 2. Structural commentary

As the title compound (I), (Fig. 1) crystallizes in a centrosymmetric space group ( $P\bar{1}$ ), the sample is racemic although the *trans* disposition of substituents about the C4—C10 bond is established. The dihedral angle between the mean planes of the five- and six-membered rings is 75.88 (8)°, while the sum of the angles about N1 is 360° within experimental error, impli-

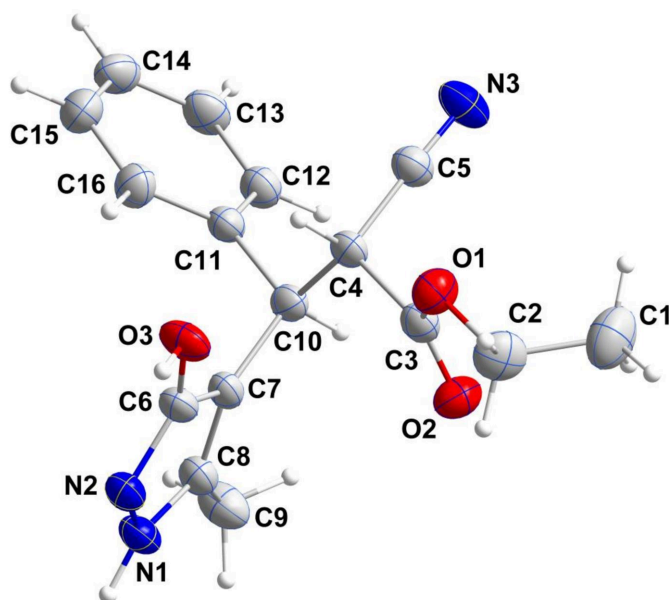


**Figure 1**  
Perspective view of the title molecule with labelling scheme and 50% probability ellipsoids.

**Table 1**  
Hydrogen-bond geometry (Å, °).

Cg1 is the centroid of the five-membered ring.

$D-H\cdots A$	$D-H$	$H\cdots A$	$D\cdots A$	$D-H\cdots A$
O3—H3 $\cdots$ N2 <sup>i</sup>	0.86 (1)	1.85 (1)	2.706 (2)	175 (3)
N1—H1 $\cdots$ N3 <sup>ii</sup>	0.91 (1)	2.13 (2)	2.948 (2)	149 (2)
C14—H14 $\cdots$ Cg1 <sup>iii</sup>	0.95	2.71	3.627 (3)	162

Symmetry codes: (i)  $-x + 1, -y + 2, -z$ ; (ii)  $x, y, z - 1$ ; (iii)  $x + 1, y, z$ .

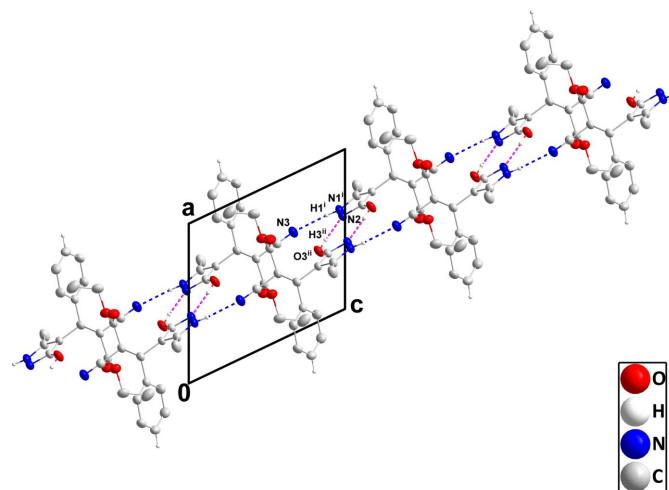
cating involvement of its lone pair in intra-ring  $\pi$  bonding. The rotational orientation of the five-membered ring may be partially determined by a C4—H4 $\cdots$ O3 hydrogen bond (H4 $\cdots$ O3 = 2.41 Å) although the C4—H4 $\cdots$ O3 angle of 115° is quite small for such an interaction.

## 3. Supramolecular features

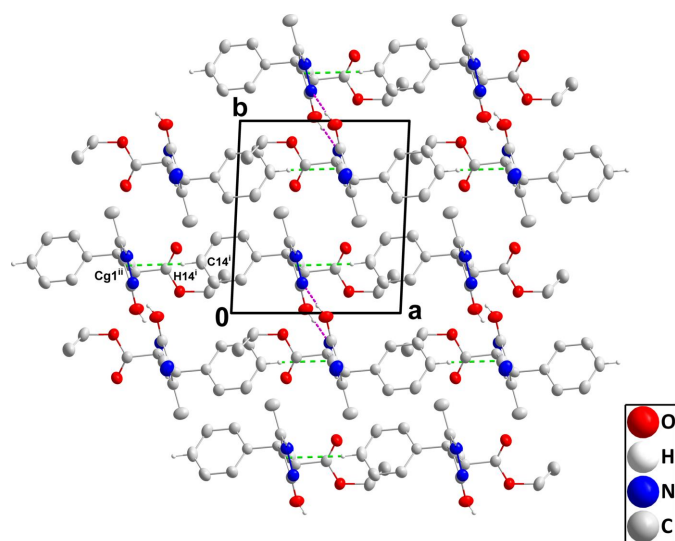
In the crystal, N1—H1 $\cdots$ N3 hydrogen bonds (Table 1) form chains of molecules extending along the *c*-axis direction that are connected by inversion-related pairs of O3—H3 $\cdots$ N2 hydrogen bonds into ribbons (Fig. 2). The ribbons are linked by C14—H14 $\cdots$ Cg1 interactions (Table 1), forming layers parallel to the *ab* plane (Fig. 3).

## 4. Hirshfeld surface analysis

In order to visualize the intermolecular interactions in the crystal of the title compound (I), a Hirshfeld surface (HS) analysis (Hirshfeld, 1977; Spackman & Jayatilaka, 2009) was carried out using *Crystal Explorer 17.5* (Turner *et al.*, 2017). In the HS plotted over  $d_{\text{norm}}$  (Fig. 4), the white surface indicates contacts with distances equal to the sum of van der Waals radii, and the red and blue colours indicate distances shorter (in close contact) or longer (distant contact) than the van der Waals radii, respectively (Venkatesan *et al.*, 2016). The bright-

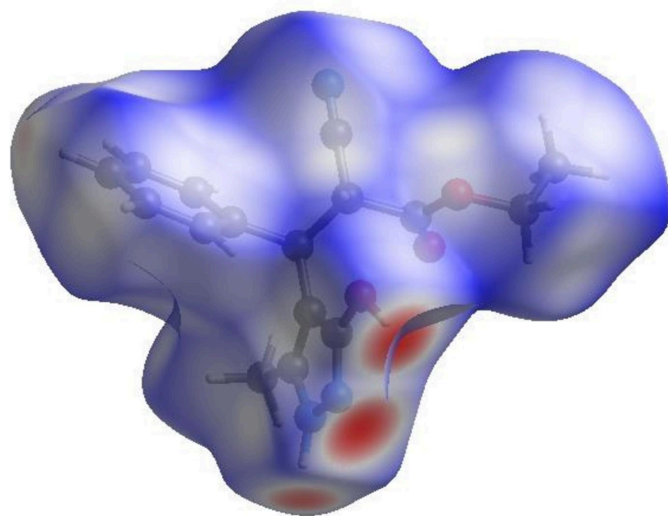


**Figure 2**  
A portion of one ribbon viewed along the *b*-axis direction with N—H $\cdots$ N and O—H $\cdots$ N hydrogen bonds depicted, respectively, by blue and dark-pink dashed lines. Hydrogen atoms not involved in these interactions are omitted for clarity. [Symmetry codes: (i)  $x, y, z + 1$ ; (ii)  $-x + 1, -y + 2, -z + 1$ .]

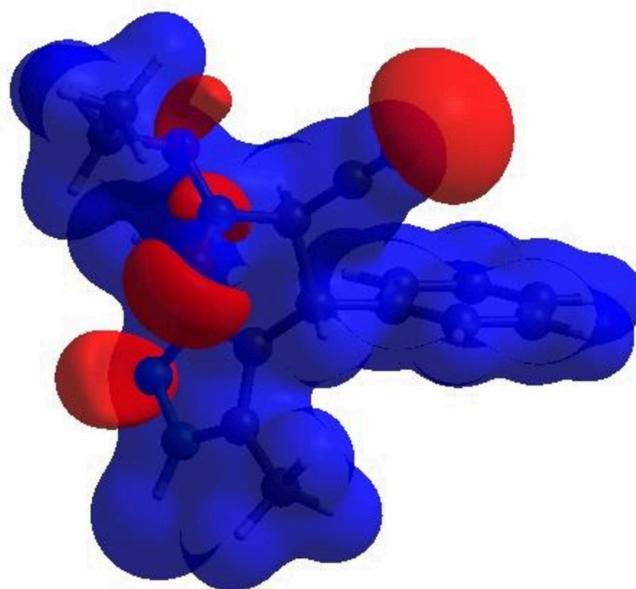


**Figure 3**  
Packing viewed along the *b*-axis direction with N–H···N and O–H···N hydrogen bonds depicted, respectively, by blue and dark-pink dashed lines while the C–H···π(*ring*) interactions are depicted by green dashed lines. Hydrogen atoms not involved in these interactions are omitted for clarity. [Symmetry codes: (i)  $-x + 1, -y + 1, -z + 1$ ; (ii)  $x - 1, y - 1, z$ ].

red spots indicate their roles as the respective donors and/or acceptors; they also appear as blue and red regions corresponding to positive and negative potentials on the HS mapped over electrostatic potential (Spackman *et al.*, 2008; Jayatilaka *et al.*, 2005) shown in Fig. 5. The blue regions indicate positive electrostatic potential (hydrogen-bond donors), while the red regions indicate negative electrostatic potential (hydrogen-bond acceptors). The shape-index of the HS is a tool to visualize  $\pi$ – $\pi$  stacking by the presence of adjacent red and blue triangles; if there are no adjacent red and/or blue triangles, then there are no  $\pi$ – $\pi$  interactions. Fig. 6 clearly suggests that there are no  $\pi$ – $\pi$  interactions in (I).

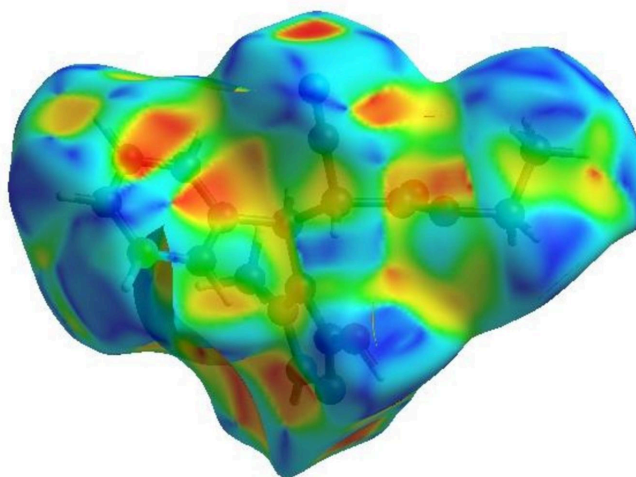


**Figure 4**  
View of the three-dimensional Hirshfeld surface of the title compound plotted over  $d_{\text{norm}}$ .

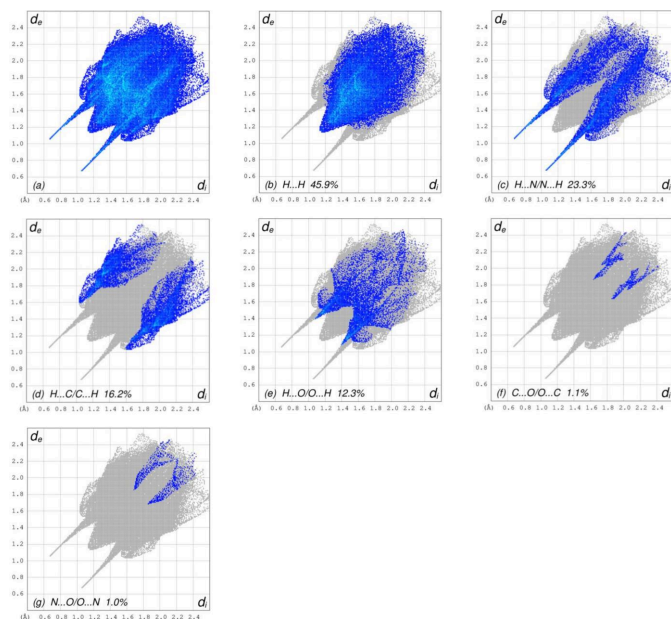


**Figure 5**  
View of the three-dimensional Hirshfeld surface of the title compound plotted over electrostatic potential energy using the STO-3 G basis set at the Hartree–Fock level of theory. Hydrogen-bond donors and acceptors are shown as blue and red regions, respectively, around the atoms corresponding to positive and negative potentials.

The overall two-dimensional fingerprint plot, Fig. 7*a*, and those delineated into H···H, H···N/N···H, H···C/C···H, H···O/O···H, C···O/O···C and N···O/O···N interactions (McKinnon *et al.*, 2007) are illustrated in Fig. 7*b–g* respectively, together with their relative contributions to the Hirshfeld surface. The most abundant interaction is H···H, contributing 45.9% to the overall crystal packing, which is reflected in Fig. 7*b* as widely scattered points of high density due to the large hydrogen content of the molecule with the tip at  $d_e = d_i = 1.15$  Å. The symmetrical pair of spikes in the fingerprint plot delineated into H···N/N···H contacts



**Figure 6**  
Hirshfeld surface of the title compound plotted over shape-index.


**Figure 7**

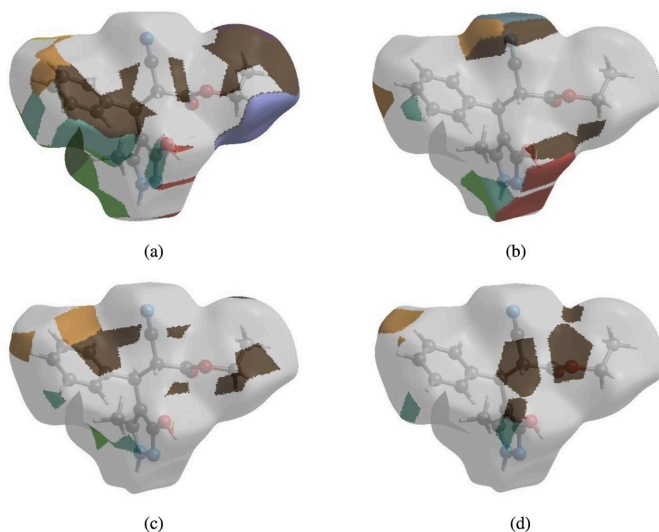
The full two-dimensional fingerprint plots for the title compound, showing (a) all interactions, and delineated into (b) H...H, (c) H...N/N...H, (d) H...C/C...H, (e) H...O/O...H, (f) C...O/O...C and (g) N...O/O...N interactions. The  $d_i$  and  $d_e$  values are the closest internal and external distances (in Å) from given points on the Hirshfeld surface.

(Fig. 7c), with a 23.3% contribution to the HS, has the tips at  $d_e + d_i = 1.72$  Å. In the presence of C—H... $\pi$  interactions, the H...C/C...H contacts, contributing 16.2% to the overall crystal packing, Fig. 7d, have the tips at  $d_e + d_i = 2.64$  Å. The symmetrical pair of spikes in the fingerprint plot delineated into H...O/O...H contacts (Fig. 7e, 12.3% contribution to the HS) has the tips at  $d_e + d_i = 2.48$  Å. Finally, the C...O/O...C (Fig. 7f) and N...O/O...N (Fig. 7g) contacts with 1.1% and 1.0% contributions, respectively, to the HS have a very low distribution of points.

The nearest neighbour coordination environment of a molecule can be determined from the colour patches on the HS based on how close to other molecules they are. The Hirshfeld surface representations with the function  $d_{\text{norm}}$  plotted onto the surface are shown for the H...H, H...N/N...H, H...C/C...H and H...O/O...H interactions in Fig. 8a–d, respectively. The Hirshfeld surface analysis confirms the importance of H-atom contacts in establishing the packing. The large number of H...H, H...N/N...H, H...C/C...H and H...O/O...H interactions suggest that van der Waals interactions and hydrogen bonding play the major roles in the crystal packing (Hathwar *et al.*, 2015).

## 5. Crystal voids

The strength of the crystal packing is important for determining the response to an applied mechanical force. If the crystal packing results in significant voids, then the molecules are not tightly packed and a small amount of applied external mechanical force may easily break the crystal. A void analysis

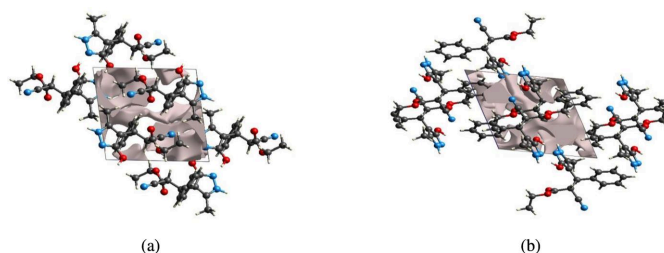

**Figure 8**

The Hirshfeld surface representations with the function fragment patch plotted onto the surface for (a) H...H, (b) H...N/N...H, (c) H...C/C...H and (d) H...O/O...H interactions.

was performed to check the mechanical stability of the crystal by adding up the electron densities of the spherically symmetric atoms contained in the asymmetric unit (Turner *et al.*, 2011). The void surface is defined as an isosurface of the procrystal electron density and is calculated for the whole unit cell where the void surface meets the boundary of the unit cell and capping faces are generated to create an enclosed volume. The volume of the crystal voids (Fig. 9a,b) and the percentage of free space in the unit cell are calculated as  $100.94$  Å<sup>3</sup> and 13.20%, respectively. Thus, the crystal packing appears compact and the mechanical stability should be substantial.

## 6. Interaction energy calculations and energy frameworks

The intermolecular interaction energies are calculated using the CE-B3LYP/6-31G(d,p) energy model available in *Crystal Explorer 17.5* (Turner *et al.*, 2017), where a cluster of molecules is generated by applying crystallographic symmetry operations with respect to a selected central molecule within the radius of 3.8 Å by default (Turner *et al.*, 2014). The total intermolecular energy ( $E_{\text{tot}}$ ) is the sum of electrostatic ( $E_{\text{ele}}$ ),


**Figure 9**

Graphical views of voids in the crystal packing of (I) (a) along the  $a$ -axis direction and (b) along the  $b$ -axis direction.

polarization ( $E_{\text{pol}}$ ), dispersion ( $E_{\text{dis}}$ ) and exchange-repulsion ( $E_{\text{rep}}$ ) energies (Turner *et al.*, 2015) with scale factors of 1.057, 0.740, 0.871 and 0.618, respectively (Mackenzie *et al.*, 2017). Hydrogen-bonding interaction energies (in  $\text{kJ mol}^{-1}$ ) were calculated to be  $-141.9$  ( $E_{\text{ele}}$ ),  $-31.4$  ( $E_{\text{pol}}$ ),  $-19.8$  ( $E_{\text{dis}}$ ),  $174.8$  ( $E_{\text{rep}}$ ) and  $-82.6$  ( $E_{\text{tot}}$ ) for  $\text{O3-H3}\cdots\text{N2}$  and  $-23.3$  ( $E_{\text{ele}}$ ),  $-3.5$  ( $E_{\text{pol}}$ ),  $-50.6$  ( $E_{\text{dis}}$ ),  $26.4$  ( $E_{\text{rep}}$ ) and  $-55.0$  ( $E_{\text{tot}}$ ) for  $\text{N1-H1}\cdots\text{N3}$ .

Energy frameworks combine the calculation of intermolecular interaction energies with a graphical representation of their magnitude (Turner *et al.*, 2015). Energies between molecular pairs are represented as cylinders joining the centroids of pairs of molecules with the cylinder radius proportional to the relative strength of the corresponding interaction energy. Energy frameworks were constructed for  $E_{\text{ele}}$  (red cylinders),  $E_{\text{dis}}$  (green cylinders) and  $E_{\text{tot}}$  (blue cylinders) (Fig. 10*a,b,c*). The evaluation of the electrostatic, dispersion and total energy frameworks indicate that the stabilization is dominated by the electrostatic energy contribution in the crystal structure of (I).

## 7. Database survey

A search of the Cambridge Structural Database (Groom *et al.*, 2016; updated to November 2023) located no other structures similar to (I) until the search fragment was simplified to (II) (Fig. 11). With this, five hits were obtained with (III) (RUWZUH; Zonouz *et al.*, 2020) being the closest match. The others are (IV) ( $R = \text{Cl}$ , IDOGUG; Elinson *et al.*, 2018*a*,  $R = \text{H}$ , FINWAD; Elinson *et al.*, 2018*b*), (V) (GEXSUA; Moghadam, 2018) and (VI) (TIWGUD; Pathak *et al.*, 2013) (Fig. 11).

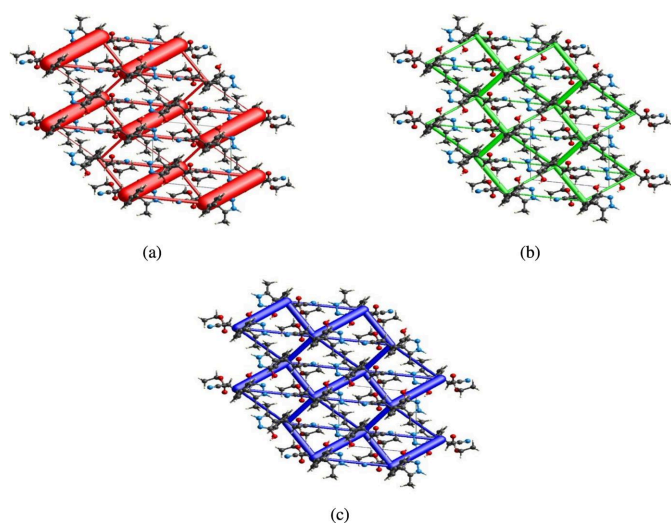


**Figure 10**

The energy frameworks for a cluster of molecules of the title compound viewed down the  $a$ -axis direction showing (a) electrostatic energy, (b) dispersion energy and (c) total energy diagrams. The cylindrical radius is proportional to the relative strength of the corresponding energies and they were adjusted to the same scale factor of 80 with cut-off value of  $5 \text{ kJ mol}^{-1}$  within  $2 \times 2 \times 2$  unit cells.

**Table 2**

Comparison of selected X-ray and DFT geometric data ( $\text{\AA}$ ,  $^\circ$ ).

Bonds/angles	X-ray	B3LYP/6-311G(d,p)
O1–C3	1.335 (2)	1.345
O1–C2	1.460 (3)	1.521
O2–C3	1.204 (2)	1.235
O3–C6	1.340 (2)	1.337
N1–C8	1.348 (3)	1.331
N1–N2	1.368 (2)	1.377
N1–H1	0.914 (10)	0.87
N2–C6	1.335 (2)	1.322
N3–C5	1.141 (3)	1.128
C3–O1–C2	116.67 (17)	115.6
C8–N1–N2	112.35 (16)	113.1
C6–N2–N1	103.86 (16)	104.6
O2–C3–O1	125.51 (19)	124.5
N2–C6–O3	122.03 (18)	123.1

## 8. DFT calculations

The theoretical optimization of the molecular structure in the gas-phase was carried out using density functional theory (DFT) with the standard B3LYP functional and 6-311G(d,p) basis-set calculations (Becke, 1993) as implemented in GAUSSIAN 09 (Frisch *et al.*, 2009). The resulting optimized parameters (bond lengths and angles) agreed satisfactorily with the experimental structural data (Table 2). The largest

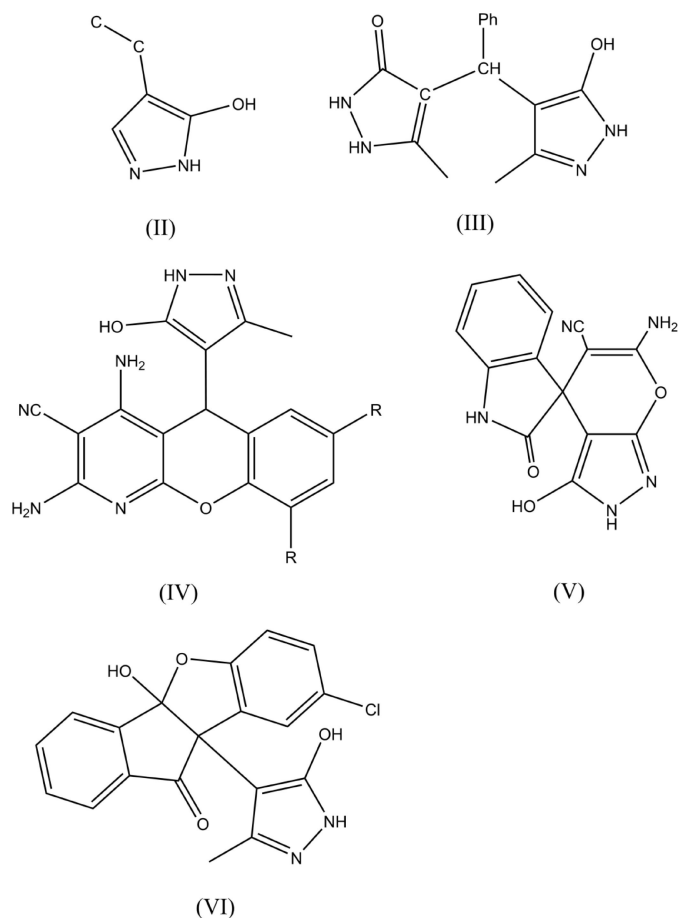


**Figure 11**

The closest matches to the title compound (I) according to the results obtained from the database survey.

**Table 3**

Calculated energies.

Molecular energy (a.u.) (eV)	Compound (I)
$E_{LUMO}$ (eV)	−0.82
$E_{HOMO}$ (eV)	−6.59
Gap $\Delta E$ (eV)	5.77
Ionization potential $I$	6.59
Electron affinity $A$	0.82
Chemical hardness $\eta$	2.88
Chemical softness $\sigma$	0.17
Electronegativity $\chi$	3.70
Chemical potential $\mu$	−3.71
Electrophilicity index $\omega$	2.38
Total energy $TE$ (eV)	−27476.33

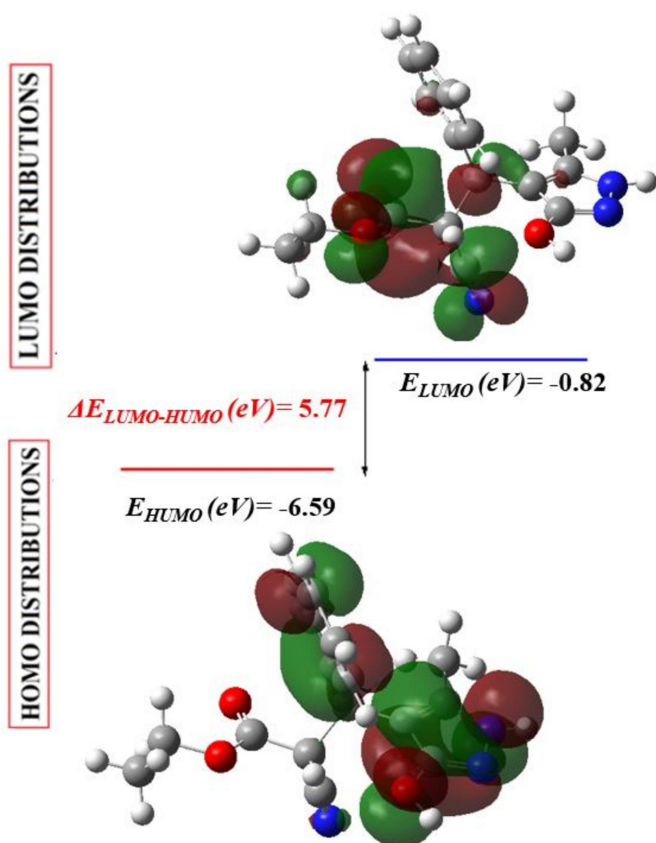
differences between the calculated and experimental values are observed for the O1–C2 (0.06 Å) and O2–C3 (0.03 Å) bond lengths and the C3–O1–C2 and N2–C6–O3 bond angle (1.07°). These disparities can be linked to the fact that these calculations relate to the isolated molecule, whereas the experimental results correspond to interacting molecules in the crystal where intra- and intermolecular interactions with neighbouring molecules are present. The highest-occupied molecular orbital (HOMO), acting as an electron donor, and the lowest-unoccupied molecular orbital (LUMO), acting as an electron acceptor, are very important parameters for quantum chemistry. When the energy gap is small, the molecule is highly polarizable and has high chemical reactivity (Elmachkouri *et al.*, 2023a). The numerical reactivity

**Table 4**

Experimental details.

Crystal data	
Chemical formula	C <sub>16</sub> H <sub>17</sub> N <sub>3</sub> O <sub>3</sub>
$M_r$	299.32
Crystal system, space group	Triclinic, $P\bar{1}$
Temperature (K)	150
$a, b, c$ (Å)	9.1397 (2), 9.4879 (2), 10.0063 (2)
$\alpha, \beta, \gamma$ (°)	79.554 (1), 63.787 (1), 83.054 (1)
$V$ (Å <sup>3</sup> )	764.75 (3)
$Z$	2
Radiation type	Cu $K\alpha$
$\mu$ (mm <sup>−1</sup> )	0.75
Crystal size (mm)	0.16 × 0.09 × 0.03
Data collection	
Diffractometer	Bruker D8 VENTURE PHOTON 3 CPAD
Absorption correction	Multi-scan ( <i>SADABS</i> ; Krause <i>et al.</i> , 2015)
$T_{min}, T_{max}$	0.88, 0.98
No. of measured, independent and observed [ $I > 2\sigma(I)$ ] reflections	36885, 2998, 2207
$R_{int}$	0.112
$(\sin \theta/\lambda)_{max}$ (Å <sup>−1</sup> )	0.618
Refinement	
$R[F^2 > 2\sigma(F^2)], wR(F^2), S$	0.048, 0.127, 1.04
No. of reflections	2998
No. of parameters	207
No. of restraints	2
H-atom treatment	H atoms treated by a mixture of independent and constrained refinement
$\Delta\rho_{max}, \Delta\rho_{min}$ (e Å <sup>−3</sup> )	0.19, −0.23

Computer programs: *APEX4* and *SAINT* (Bruker, 2021), *SHELXT* (Sheldrick, 2015a), *SHELXL2019/1* (Sheldrick, 2015b), *DIAMOND* (Brandenburg & Putz, 2012) and *SHELXTL* (Sheldrick, 2008).


**Figure 12**

The energy band gap of the title compound.

descriptors (ionization potential, electron affinity, chemical hardness, chemical softness, electronegativity, chemical potential, electrophilicity index and total energy), which are mainly based on the HOMO–LUMO energies, are summarized in Table 3. The optimized frontier molecular orbitals (HOMO and LUMO) are shown in Fig. 12. The LUMO is mainly centered on the 2-cyano group and spans the entire ethyl propanoate chain while the HOMO is primarily centered on the 3-phenyl substituent and spans the 3-(3-hydroxy-5-methyl-1*H*-pyrazol-4-yl) portion. The energy band gap [ $E = E_{LUMO} - E_{HOMO}$ ] of the molecule is about 5.77 eV, and the frontier molecular orbital energies,  $E_{HOMO}$  and  $E_{LUMO}$ , are −6.59 eV and −0.82 eV, respectively.

## 9. Synthesis and crystallization

To a solution of pyrazolone (4 mmol), benzaldehyde (4 mmol) and ethyl 2-cyanoacetate (4 mmol, 0.42 ml) in absolute ethanol (12 ml), were added two drops of piperidine and the reaction mixture was refluxed with magnetic stirring for 2 h. The progress of the reaction was monitored by TLC using an ethyl acetate/hexane mixture as eluant. Finally, the resulting precipitate was filtered and the isolated solid was purified by recrystallization from ethanol to afford colourless crystals in 96% yield. The melting point was 454 K.

## 10. Refinement

Crystal data, data collection and structure refinement details are summarized in Table 4. Hydrogen atoms attached to carbon were included as riding contributions in idealized positions with isotropic displacement parameters tied to those of the attached atoms while those attached to nitrogen and to oxygen were located in a difference map and refined with DFIX 0.91 0.01 and DFIX 0.85 0.01 instructions, respectively.

## Funding information

The support of NSF-MRI grant No.1228232 for the purchase of the diffractometer and Tulane University for support of the Tulane Crystallography Laboratory are gratefully acknowledged. TH is grateful to Hacettepe University Scientific Research Project Unit (grant No. 013 D04 602 004).

## References

Ait Elmachkouri, Y., Irrou, E., Thiruvalluvar, A. A., Anouar, E. H., Varadharajan, V., Ouachtak, H., Mague, J. T., Sebbar, N. K., Essassi, E. M. & Labd Taha, M. (2023a). *J. Biomol. Struct. Dyn.* <https://doi.org/10.1080/10406638.2023.2219804>.

Ait Elmachkouri, Y., Sert, Y., Irrou, E., Anouar, E. H., Ouachtak, H., Mague, J. T., Sebbar, N. K., Essassi, E. M. & Labd Taha, M. (2023b). *Polycyclic Aromat. Compd.* <https://doi.org/10.1080/07391102.2023.2268187>.

Akbas, E., Berber, I., Sener, A. & Hasanov, B. (2005). *Farmaco*, **60**, 23–26.

Becke, A. D. (1993). *J. Chem. Phys.* **98**, 5648–5652.

Bensaber, S. M., Allafe, H. A., Ermeli, N. B., Mohamed, S. B., Zetrini, A. A., Alsabri, S. G., Erhuma, M., Hermann, A., Jaeda, M. I. & Gbaj, A. M. (2014). *Med. Chem. Res.* **23**, 5120–5134.

Brandenburg, K. & Putz, H. (2012). *DIAMOND*. Crystal Impact GbR, Bonn, Germany.

Bruker (2021). *APEX4* and *SAINT*. Bruker AXS, Madison, Wisconsin, USA.

Elinson, N. E., Vereshchagin, A. N., Anisina, Yu. E., Fakhrutdinov, A. N., Goloveshkin, A. S. & Egorov, M. P. (2018a). *J. Fluor. Chem.* **213**, 31–36.

Elinson, N. E., Vereshchagin, A. N., Anisina, Yu. E., Goloveshkin, A. S., Ushakov, I. E. & Egorov, M. P. (2018b). *Mendeleev Commun.* **28**, 372–374.

Elmachkouri, Y. A., Irrou, E., Dalbouha, S., Ouachtak, H., Mague, J. T., Hökelek, T., El Ghayati, L., Sebbar, N. K. & Taha, M. L. (2022). *Acta Cryst. E78*, 1265–1270.

Frisch, M. J., Trucks, G. W., Schlegel, H. B., Scuseria, G. E., Robb, M. A., Cheeseman, J. R., Scalmani, G., Barone, V., Mennucci, B., Petersson, G. A., Nakatsuji, H., Caricato, M., Li, X., Hratchian, H. P., Izmaylov, A. F., Bloino, J., Zheng, G., Sonnenberg, J. L., Hada, M., Ehara, M., Toyota, K., Fukuda, R., Hasegawa, J., Ishida, M., Nakajima, T., Honda, Y., Kitao, O., Nakai, H., Vreven, T., Montgomery, J. A. Jr, Peralta, J. E., Ogliaro, F., Bearpark, M., Heyd, J. J., Brothers, E., Kudin, K. N., Staroverov, V. N., Kobayashi, R., Normand, J., Raghavachari, K., Rendell, A., Burant, J. C., Iyengar, S. S., Tomasi, J., Cossi, M., Rega, N., Millam, J. M., Klene, M., Knox,

J. E., Cross, J. B., Bakken, V., Adamo, C., Jaramillo, J., Gomperts, R., Stratmann, R. E., Yazyev, O., Austin, A. J., Cammi, R., Pomelli, C., Ochterski, J. W., Martin, R. L., Morokuma, K., Zakrzewski, V. G., Voth, G. A., Salvador, P., Dannenberg, J. J., Dapprich, S., Daniels, A. D., Farkas, O., Foresman, J. B., Ortiz, J. V., Cioslowski, J. & Fox, D. J. (2009). *GAUSSIAN09*. Gaussian Inc., Wallingford, CT, US.

Groom, C. R., Bruno, I. J., Lightfoot, M. P. & Ward, S. C. (2016). *Acta Cryst. B72*, 171–179.

Gürsoy, A., Demirayak, S., Capan, G., Erol, K. & Vural, K. (2000). *Eur. J. Med. Chem.* **35**, 359–364.

Hathwar, V. R., Sist, M., Jørgensen, M. R. V., Mamakhel, A. H., Wang, X., Hoffmann, C. M., Sugimoto, K., Overgaard, J. & Iversen, B. B. (2015). *IUCrJ*, **2**, 563–574.

Hirshfeld, H. L. (1977). *Theor. Chim. Acta*, **44**, 129–138.

Irrou, E., Elmachkouri, Y. A., Oubella, A., Ouchtak, H., Dalbouha, S., Mague, J. T., Hökelek, T., El Ghayati, L., Sebbar, N. K. & Taha, M. L. (2022). *Acta Cryst. E78*, 953–960.

Jayatilaka, D., Grimwood, D. J., Lee, A., Lemay, A., Russel, A. J., Taylor, C., Wolff, S. K., Cassam-Chenai, P. & Whitton, A. (2005). *TONTO - A System for Computational Chemistry*. Available at: <http://hirshfeldsurface.net/>

Krause, L., Herbst-Irmer, R., Sheldrick, G. M. & Stalke, D. (2015). *J. Appl. Cryst.* **48**, 3–10.

Mackenzie, C. F., Spackman, P. R., Jayatilaka, D. & Spackman, M. A. (2017). *IUCrJ*, **4**, 575–587.

McKinnon, J. J., Jayatilaka, D. & Spackman, M. A. (2007). *Chem. Commun.* pp. 3814–3816.

Moghadam, M. (2018). *CSD Communication* (refcode GEXSUA). CCDC, Cambridge, England.

Moukha-Chafiq, O., Taha, M. L., Lazrek, H. B., Vasseur, J. J. & Clercq, E. D. (2006). *Nucleosides Nucleotides Nucleic Acids*, **25**, 849–860.

Moukha-chafiq, O., Taha, M. L. & Mouna, A. (2007a). *Nucleosides Nucleotides Nucleic Acids*, **26**, 1107–1110.

Moukha-Chafiq, O., Taha, M. L., Mouna, A., Lazrek, H. B., Vasseur, J. J. & De Clercq, E. (2007b). *Nucleosides Nucleotides Nucleic Acids*, **26**, 335–345.

Pathak, S., Debnath, K., Hossain, S. T., Mukherjee, S. K. & Pramanik, A. (2013). *Tetrahedron Lett.* **54**, 3137–3143.

Prasath, R., Bhavana, P., Sarveswari, S., Ng, S. W. & Tiekink, E. R. T. (2015). *J. Mol. Struct.* **1081**, 201–210.

Sheldrick, G. M. (2015a). *Acta Cryst. A71*, 3–8.

Sheldrick, G. M. (2015b). *Acta Cryst. C71*, 3–8.

Spackman, M. A. & Jayatilaka, D. (2009). *CrystEngComm*, **11**, 19–32.

Spackman, M. A., McKinnon, J. J. & Jayatilaka, D. (2008). *CrystEngComm*, **10**, 377–388.

Turner, M. J., Grabowsky, S., Jayatilaka, D. & Spackman, M. A. (2014). *J. Phys. Chem. Lett.* **5**, 4249–4255.

Turner, M. J., McKinnon, J. J., Jayatilaka, D. & Spackman, M. A. (2011). *CrystEngComm*, **13**, 1804–1813.

Turner, M. J., McKinnon, J. J., Wolff, S. K., Grimwood, D. J., Spackman, P. R., Jayatilaka, D. & Spackman, M. A. (2017). *CrystalExplorer17*. The University of Western Australia.

Turner, M. J., Thomas, S. P., Shi, M. W., Jayatilaka, D. & Spackman, M. A. (2015). *Chem. Commun.* **51**, 3735–3738.

Venkatesan, P., Thamotharan, S., Ilangovan, A., Liang, H. & Sundius, T. (2016). *Spectrochim. Acta A Mol. Biomol. Spectrosc.* **153**, 625–636.

Zonouz, A. M., Beiranvand, M., Mohammad-Rezaei, R. & Naderi, S. (2020). *Lett. Org. Chem.* **17**, 548–554.

## supporting information

*Acta Cryst.* (2024). E80, 240-246 [https://doi.org/10.1107/S2056989024000744]

## Crystal structure, Hirshfeld surface analysis, crystal voids, interaction energy calculations and energy frameworks and DFT calculations of ethyl 2-cyano-3-(3-hydroxy-5-methyl-1*H*-pyrazol-4-yl)-3-phenylpropanoate

Younesse Ait Elmachkouri, Ezaddine Irrou, Hanae El Monfalouti, Ahmed Mazzah, Tuncer Hökelek, Joel T. Mague, Mohamed Labd Taha and Nada Kheira Sebbar

### Computing details

#### Ethyl 2-cyano-3-(3-hydroxy-5-methyl-1*H*-pyrazol-4-yl)-3-phenylpropanoate

##### Crystal data

$C_{16}H_{17}N_3O_3$	$Z = 2$
$M_r = 299.32$	$F(000) = 316$
Triclinic, $P\bar{1}$	$D_x = 1.300 \text{ Mg m}^{-3}$
$a = 9.1397 (2) \text{ \AA}$	Cu $K\alpha$ radiation, $\lambda = 1.54178 \text{ \AA}$
$b = 9.4879 (2) \text{ \AA}$	Cell parameters from 8141 reflections
$c = 10.0063 (2) \text{ \AA}$	$\theta = 4.7\text{--}72.2^\circ$
$\alpha = 79.554 (1)^\circ$	$\mu = 0.75 \text{ mm}^{-1}$
$\beta = 63.787 (1)^\circ$	$T = 150 \text{ K}$
$\gamma = 83.054 (1)^\circ$	Prism, clear colourless
$V = 764.75 (3) \text{ \AA}^3$	$0.16 \times 0.09 \times 0.03 \text{ mm}$

##### Data collection

Bruker D8 VENTURE PHOTON 3 CPAD diffractometer	$T_{\min} = 0.88, T_{\max} = 0.98$
Radiation source: INCOATEC $I\mu\text{S}$ micro-focus source	36885 measured reflections
Mirror monochromator	2998 independent reflections
Detector resolution: $7.3910 \text{ pixels mm}^{-1}$	2207 reflections with $I > 2\sigma(I)$
$\varphi$ and $\omega$ scans	$R_{\text{int}} = 0.112$
Absorption correction: multi-scan ( <i>SADABS</i> ; Krause <i>et al.</i> , 2015)	$\theta_{\max} = 72.4^\circ, \theta_{\min} = 4.7^\circ$
	$h = -11 \rightarrow 11$
	$k = -11 \rightarrow 11$
	$l = -12 \rightarrow 12$

##### Refinement

Refinement on $F^2$	Secondary atom site location: difference Fourier map
Least-squares matrix: full	Hydrogen site location: mixed
$R[F^2 > 2\sigma(F^2)] = 0.048$	H atoms treated by a mixture of independent and constrained refinement
$wR(F^2) = 0.127$	$w = 1/[\sigma^2(F_o^2) + (0.0565P)^2 + 0.3004P]$
$S = 1.04$	where $P = (F_o^2 + 2F_c^2)/3$
2998 reflections	$(\Delta/\sigma)_{\max} < 0.001$
207 parameters	$\Delta\rho_{\max} = 0.19 \text{ e \AA}^{-3}$
2 restraints	$\Delta\rho_{\min} = -0.23 \text{ e \AA}^{-3}$
Primary atom site location: dual	

*Special details*

**Experimental.** The diffraction data were obtained from sets of frames, each of width  $0.5^\circ$  in  $\omega$  or  $\varphi$ , collected with scan parameters determined by the "strategy" routine in *APEX4*. The scan time was sec/frame.

**Geometry.** All esds (except the esd in the dihedral angle between two l.s. planes) are estimated using the full covariance matrix. The cell esds are taken into account individually in the estimation of esds in distances, angles and torsion angles; correlations between esds in cell parameters are only used when they are defined by crystal symmetry. An approximate (isotropic) treatment of cell esds is used for estimating esds involving l.s. planes.

**Refinement.** Refinement of  $F^2$  against ALL reflections. The weighted R-factor wR and goodness of fit S are based on  $F^2$ , conventional R-factors R are based on F, with F set to zero for negative  $F^2$ . The threshold expression of  $F^2 > 2\sigma(F^2)$  is used only for calculating R-factors(gt) etc. and is not relevant to the choice of reflections for refinement. R-factors based on  $F^2$  are statistically about twice as large as those based on F, and R-factors based on ALL data will be even larger. H-atoms attached to carbon were placed in calculated positions (C—H = 0.95 - 1.00 Å) and were included as riding contributions with isotropic displacement parameters 1.2 - 1.5 times those of the attached atoms. Those attached to nitrogen and to oxygen were placed in locations derived from a difference map and refined with DFIX 0.91 0.01 and DFIX 0.85 0.01 instructions, respectively.

*Fractional atomic coordinates and isotropic or equivalent isotropic displacement parameters ( $\text{\AA}^2$ )*

	<i>x</i>	<i>y</i>	<i>z</i>	$U_{\text{iso}}^*/U_{\text{eq}}$
O1	0.31072 (17)	0.88849 (16)	0.53196 (17)	0.0374 (4)
O2	0.34195 (18)	0.66225 (16)	0.47923 (18)	0.0396 (4)
O3	0.5608 (2)	0.97967 (16)	0.16765 (17)	0.0380 (4)
H3	0.510 (3)	1.038 (2)	0.124 (3)	0.057*
N1	0.6348 (2)	0.70329 (19)	-0.03454 (19)	0.0340 (4)
H1	0.641 (3)	0.670 (3)	-0.1172 (19)	0.051*
N2	0.5886 (2)	0.84391 (19)	-0.01623 (19)	0.0327 (4)
N3	0.6355 (2)	0.7145 (2)	0.6688 (2)	0.0441 (5)
C1	0.0507 (3)	0.8091 (3)	0.7386 (3)	0.0574 (7)
H1A	-0.067805	0.824670	0.774657	0.086*
H1B	0.085342	0.844719	0.805661	0.086*
H1C	0.079772	0.706292	0.737677	0.086*
C2	0.1346 (3)	0.8881 (3)	0.5822 (3)	0.0453 (6)
H2A	0.112275	0.842376	0.512074	0.054*
H2B	0.089410	0.988276	0.579737	0.054*
C3	0.3974 (2)	0.7698 (2)	0.4823 (2)	0.0306 (4)
C4	0.5793 (2)	0.7876 (2)	0.4307 (2)	0.0278 (4)
H4	0.604261	0.890474	0.389034	0.033*
C5	0.6124 (2)	0.7486 (2)	0.5641 (2)	0.0333 (5)
C6	0.5994 (2)	0.8562 (2)	0.1099 (2)	0.0301 (4)
C7	0.6532 (2)	0.7267 (2)	0.1720 (2)	0.0278 (4)
C8	0.6750 (2)	0.6317 (2)	0.0746 (2)	0.0316 (4)
C9	0.7316 (3)	0.4776 (2)	0.0780 (3)	0.0443 (6)
H9A	0.680821	0.428399	0.032257	0.066*
H9B	0.700504	0.432922	0.182580	0.066*
H9C	0.850573	0.470104	0.021522	0.066*
C10	0.6881 (2)	0.6924 (2)	0.3084 (2)	0.0277 (4)
H10	0.660923	0.590388	0.352463	0.033*
C11	0.8671 (2)	0.7065 (2)	0.2704 (2)	0.0276 (4)
C12	0.9482 (2)	0.5996 (2)	0.3305 (2)	0.0335 (5)

H12	0.892943	0.516295	0.391447	0.040*
C13	1.1095 (3)	0.6133 (3)	0.3023 (2)	0.0391 (5)
H13	1.163765	0.539442	0.343921	0.047*
C14	1.1906 (3)	0.7340 (3)	0.2139 (3)	0.0410 (5)
H14	1.300235	0.744139	0.195775	0.049*
C15	1.1118 (3)	0.8403 (3)	0.1519 (3)	0.0399 (5)
H15	1.168056	0.922894	0.090037	0.048*
C16	0.9514 (3)	0.8269 (2)	0.1793 (2)	0.0356 (5)
H16	0.898446	0.900196	0.135782	0.043*

*Atomic displacement parameters (Å<sup>2</sup>)*

	$U^{11}$	$U^{22}$	$U^{33}$	$U^{12}$	$U^{13}$	$U^{23}$
O1	0.0302 (8)	0.0378 (8)	0.0425 (9)	0.0015 (6)	-0.0144 (6)	-0.0070 (7)
O2	0.0342 (8)	0.0396 (9)	0.0476 (9)	-0.0058 (6)	-0.0179 (7)	-0.0090 (7)
O3	0.0555 (10)	0.0341 (8)	0.0356 (8)	0.0037 (7)	-0.0318 (7)	-0.0034 (6)
N1	0.0400 (10)	0.0407 (10)	0.0253 (8)	-0.0016 (7)	-0.0176 (7)	-0.0055 (7)
N2	0.0360 (9)	0.0390 (10)	0.0265 (8)	-0.0032 (7)	-0.0173 (7)	-0.0013 (7)
N3	0.0489 (12)	0.0569 (13)	0.0323 (10)	0.0084 (9)	-0.0241 (9)	-0.0097 (9)
C1	0.0411 (14)	0.0526 (16)	0.0616 (17)	-0.0039 (11)	-0.0058 (12)	-0.0099 (13)
C2	0.0330 (12)	0.0523 (14)	0.0522 (14)	0.0081 (10)	-0.0198 (10)	-0.0138 (11)
C3	0.0314 (10)	0.0362 (11)	0.0256 (10)	-0.0001 (8)	-0.0145 (8)	-0.0027 (8)
C4	0.0304 (10)	0.0312 (10)	0.0241 (9)	-0.0026 (8)	-0.0148 (8)	-0.0003 (8)
C5	0.0320 (11)	0.0404 (12)	0.0294 (10)	0.0002 (8)	-0.0150 (9)	-0.0061 (9)
C6	0.0312 (10)	0.0385 (11)	0.0245 (9)	-0.0039 (8)	-0.0154 (8)	-0.0035 (8)
C7	0.0264 (9)	0.0358 (11)	0.0218 (9)	-0.0037 (7)	-0.0117 (7)	-0.0004 (8)
C8	0.0333 (10)	0.0367 (11)	0.0257 (9)	-0.0043 (8)	-0.0143 (8)	-0.0011 (8)
C9	0.0606 (15)	0.0409 (13)	0.0370 (12)	0.0051 (11)	-0.0265 (11)	-0.0095 (10)
C10	0.0319 (10)	0.0275 (10)	0.0264 (9)	-0.0037 (7)	-0.0161 (8)	0.0004 (8)
C11	0.0291 (10)	0.0324 (10)	0.0232 (9)	-0.0018 (8)	-0.0127 (8)	-0.0041 (8)
C12	0.0349 (11)	0.0376 (12)	0.0291 (10)	-0.0014 (9)	-0.0160 (9)	-0.0017 (9)
C13	0.0340 (11)	0.0511 (14)	0.0359 (11)	0.0050 (9)	-0.0204 (9)	-0.0054 (10)
C14	0.0293 (11)	0.0595 (15)	0.0378 (12)	-0.0053 (10)	-0.0152 (9)	-0.0119 (10)
C15	0.0380 (12)	0.0437 (13)	0.0374 (12)	-0.0119 (10)	-0.0146 (9)	-0.0021 (10)
C16	0.0359 (11)	0.0360 (12)	0.0346 (11)	-0.0048 (9)	-0.0167 (9)	0.0019 (9)

*Geometric parameters (Å, °)*

O1—C3	1.335 (2)	C6—C7	1.409 (3)
O1—C2	1.460 (3)	C7—C8	1.380 (3)
O2—C3	1.204 (2)	C7—C10	1.506 (3)
O3—C6	1.340 (2)	C8—C9	1.490 (3)
O3—H3	0.857 (10)	C9—H9A	0.9800
N1—C8	1.348 (3)	C9—H9B	0.9800
N1—N2	1.370 (2)	C9—H9C	0.9800
N1—H1	0.914 (10)	C10—C11	1.524 (3)
N2—C6	1.335 (2)	C10—H10	1.0000
N3—C5	1.141 (3)	C11—C12	1.389 (3)

C1—C2	1.501 (4)	C11—C16	1.394 (3)
C1—H1A	0.9800	C12—C13	1.391 (3)
C1—H1B	0.9800	C12—H12	0.9500
C1—H1C	0.9800	C13—C14	1.379 (3)
C2—H2A	0.9900	C13—H13	0.9500
C2—H2B	0.9900	C14—C15	1.383 (3)
C3—C4	1.529 (3)	C14—H14	0.9500
C4—C5	1.470 (3)	C15—C16	1.385 (3)
C4—C10	1.552 (3)	C15—H15	0.9500
C4—H4	1.0000	C16—H16	0.9500
C3—O1—C2	116.68 (17)	N1—C8—C7	107.38 (18)
C6—O3—H3	109.6 (19)	N1—C8—C9	122.35 (18)
C8—N1—N2	112.28 (16)	C7—C8—C9	130.27 (18)
C8—N1—H1	127.6 (17)	C8—C9—H9A	109.5
N2—N1—H1	120.0 (17)	C8—C9—H9B	109.5
C6—N2—N1	103.85 (16)	H9A—C9—H9B	109.5
C2—C1—H1A	109.5	C8—C9—H9C	109.5
C2—C1—H1B	109.5	H9A—C9—H9C	109.5
H1A—C1—H1B	109.5	H9B—C9—H9C	109.5
C2—C1—H1C	109.5	C7—C10—C11	112.75 (16)
H1A—C1—H1C	109.5	C7—C10—C4	111.51 (16)
H1B—C1—H1C	109.5	C11—C10—C4	109.52 (15)
O1—C2—C1	111.9 (2)	C7—C10—H10	107.6
O1—C2—H2A	109.2	C11—C10—H10	107.6
C1—C2—H2A	109.2	C4—C10—H10	107.6
O1—C2—H2B	109.2	C12—C11—C16	118.64 (18)
C1—C2—H2B	109.2	C12—C11—C10	119.87 (17)
H2A—C2—H2B	107.9	C16—C11—C10	121.46 (18)
O2—C3—O1	125.49 (19)	C11—C12—C13	120.77 (19)
O2—C3—C4	123.93 (19)	C11—C12—H12	119.6
O1—C3—C4	110.57 (17)	C13—C12—H12	119.6
C5—C4—C3	107.30 (16)	C14—C13—C12	120.0 (2)
C5—C4—C10	110.20 (16)	C14—C13—H13	120.0
C3—C4—C10	112.11 (15)	C12—C13—H13	120.0
C5—C4—H4	109.1	C13—C14—C15	119.8 (2)
C3—C4—H4	109.1	C13—C14—H14	120.1
C10—C4—H4	109.1	C15—C14—H14	120.1
N3—C5—C4	177.9 (2)	C14—C15—C16	120.4 (2)
N2—C6—O3	122.06 (18)	C14—C15—H15	119.8
N2—C6—C7	112.33 (18)	C16—C15—H15	119.8
O3—C6—C7	125.61 (17)	C15—C16—C11	120.4 (2)
C8—C7—C6	104.16 (17)	C15—C16—H16	119.8
C8—C7—C10	125.22 (18)	C11—C16—H16	119.8
C6—C7—C10	130.58 (18)		
C8—N1—N2—C6	-0.9 (2)	C8—C7—C10—C11	83.8 (2)
C3—O1—C2—C1	79.9 (2)	C6—C7—C10—C11	-93.6 (2)

C2—O1—C3—O2	-1.9 (3)	C8—C7—C10—C4	-152.51 (19)
C2—O1—C3—C4	178.73 (17)	C6—C7—C10—C4	30.1 (3)
O2—C3—C4—C5	-93.5 (2)	C5—C4—C10—C7	178.19 (16)
O1—C3—C4—C5	85.9 (2)	C3—C4—C10—C7	58.8 (2)
O2—C3—C4—C10	27.6 (3)	C5—C4—C10—C11	-56.3 (2)
O1—C3—C4—C10	-152.99 (16)	C3—C4—C10—C11	-175.76 (15)
N1—N2—C6—O3	-178.86 (18)	C7—C10—C11—C12	-133.87 (19)
N1—N2—C6—C7	0.7 (2)	C4—C10—C11—C12	101.4 (2)
N2—C6—C7—C8	-0.2 (2)	C7—C10—C11—C16	47.9 (3)
O3—C6—C7—C8	179.32 (19)	C4—C10—C11—C16	-76.9 (2)
N2—C6—C7—C10	177.66 (19)	C16—C11—C12—C13	1.0 (3)
O3—C6—C7—C10	-2.8 (3)	C10—C11—C12—C13	-177.28 (18)
N2—N1—C8—C7	0.9 (2)	C11—C12—C13—C14	0.0 (3)
N2—N1—C8—C9	-179.08 (19)	C12—C13—C14—C15	-0.9 (3)
C6—C7—C8—N1	-0.4 (2)	C13—C14—C15—C16	0.7 (3)
C10—C7—C8—N1	-178.39 (17)	C14—C15—C16—C11	0.3 (3)
C6—C7—C8—C9	179.5 (2)	C12—C11—C16—C15	-1.2 (3)
C10—C7—C8—C9	1.5 (3)	C10—C11—C16—C15	177.08 (19)

#### Hydrogen-bond geometry ( $\text{\AA}$ , $^\circ$ )

Cg1 is the centroid of the five-membered ring.

$D-H\cdots A$	$D-H$	$H\cdots A$	$D\cdots A$	$D-H\cdots A$
O3—H3 $\cdots$ N2 <sup>i</sup>	0.86 (1)	1.85 (1)	2.706 (2)	175 (3)
N1—H1 $\cdots$ N3 <sup>ii</sup>	0.91 (1)	2.13 (2)	2.948 (2)	149 (2)
C14—H14 $\cdots$ Cg1 <sup>iii</sup>	0.95	2.71	3.627 (3)	162

Symmetry codes: (i)  $-x+1, -y+2, -z$ ; (ii)  $x, y, z-1$ ; (iii)  $x+1, y, z$ .